Clues on void evolution – I. Large-scale galaxy distributions around voids

L. Ceccarelli,[1,2]⋆ D. Paz,[1,2] M. Lares,[1,2] N. Padilla[3] and D. García Lambas[1,2]

[1]*Instituto de Astronomía Teórica y Experimental, UNC-CONICET, X5000BGR, Córdoba, Argentina*
[2]*Observatorio Astronómico de Córdoba, UNC, X5000BGR, Córdoba, Argentina*
[3]*Departamento de Astronomía y Astrofísica, Pontificia Universidad Católica de Chile, Santiago, Chile*

ABSTRACT

We perform a statistical study focused on void environments. We examine galaxy density profiles around voids in the Sloan Digital Sky Survey (SDSS), finding a correlation between void-centric distance to the shell of maximum density and void radius when a maximum in overdensity exists. We analyse voids with and without a surrounding overdense shell in the SDSS. We find that small voids are more frequently surrounded by overdense shells whereas the radial galaxy density profile of large voids tends to rise smoothly towards the mean galaxy density. We analyse the fraction of voids surrounded by overdense shells finding a continuous trend with void radius. The differences between voids with and without an overdense shell around them can be understood in terms of whether the voids are, on average, in the process of collapsing or continuing their expansion, respectively, in agreement with previous theoretical expectations. We use numerical simulations coupled to semi-analytic models of galaxy formation in order to test and interpret our results. The very good agreement between the mock catalogue results and the observations provides additional support to the viability of a Λ cold dark matter model to reproduce the large-scale structure of the Universe as defined by the void network, in a way which has not been analysed previously.

Key words: methods: data analysis – methods: observational – methods: statistical – large-scale structure of Universe.

1 INTRODUCTION

Although the large-scale galaxy and matter distributions are dominated by different structures such as groups, clusters, filaments, walls, etc., most of the volume of the Universe is occupied by voids: large underdense regions are the prominent structures at large scales.

These large-scale underdensities have been identified and analysed in numerical simulations and in galaxy catalogues (Hoffman & Shaham 1982; Hausman, Olson & Roth 1983; Fillmore & Goldreich 1984; Icke 1984; Bertschinger 1985; Pellegrini, da Costa & de Carvalho 1989; Kauffmann & Fairall 1991; Blumenthal et al. 1992; Slezak, de Lapparent & Bijaoui 1993; El-Ad & Piran 1997, 2000; El-Ad, Piran & Dacosta 1997; Aikio & Maehoenen 1998; Müller et al. 2000; Hoyle & Vogeley 2002, 2004; Plionis & Basilakos 2002; Sheth & van de Weygaert 2004; Ceccarelli et al. 2006; Furlanetto & Piran 2006; Patiri et al. 2006; Tikhonov 2006; Neyrinck 2008; Aragon-Calvo et al. 2010; Pan et al. 2012; Sutter et al. 2012a). Despite the fact that the agreement between void finders is weaker for small- and medium-scale voids, to a first approximation their more prominent properties are similar. In general, similar properties of voids are found regardless of the diversity of identification methods

and galaxy sample properties. For a comparison of the different techniques adopted see Colberg et al. (2008).

It is also important to stress the fact that galaxies and haloes trace the void distribution in a similar fashion. Padilla, Ceccarelli & Lambas (2005) have studied voids defined by the spatial distribution of haloes and galaxies finding that they have comparable general statistical and dynamical properties, such as abundances, correlation functions and velocity fields.

Moreover, the statistics of void and matter distributions are strongly related (White 1979) and therefore voids can provide simple and useful information on the clustering pattern, giving clues on the formation and evolution of overdense structures. Observations of the large-scale structure traced by voids can also be used to constrain cosmological models (e.g. Peebles 2001; Kolokotronis, Basilakos & Plionis 2002; Benson et al. 2003; Colberg et al. 2005b; Biswas, Alizadeh & Wandelt 2010; Lavaux & Wandelt 2010; Bos et al. 2012a,b; Hernandez-Monteagudo & Smith 2012; Park et al. 2012; Sutter et al. 2012b; Clampitt, Cai & Li 2013) and to shed light on the mechanisms of galaxy evolution and its dependence on the large-scale environment (Hahn et al. 2007a,b; Ceccarelli, Padilla & Lambas 2008; Ceccarelli et al. 2012; Lietzen et al. 2012).

Voids in the galaxy distribution, in a first approximation, can be described as simple underdense regions which have nearly spherical shapes and isotropic expansion motions (Icke 1984;

⋆ E-mail: ceccarelli@oac.uncor.edu

van de Weygaert & Bertschinger 1996; Padilla et al. 2005; Ceccarelli et al. 2006). Nevertheless, in more detailed analyses it became clear that as voids are not isolated structures but rather part of an intricate network, their structure and dynamics are more complicated (Bertschinger 1985; Melott & Shandarin 1990; Mathis & White 2002; Colberg, Krughoff & Connolly 2005a; Shandarin et al. 2006; Platen, van de Weygaert & Jones 2008; Aragon-Calvo & Szalay 2013). The formation and evolution of voids is strongly affected by their surrounding large-scale environment (Sheth & van de Weygaert 2004). The void distribution also evolves accordingly, as matter collapses to form structures and galaxies dissipate from voids, making a supercluster–void network (Einasto et al. 1997, 2012; Frisch et al. 1995). In order to deepen our understanding of the nature of voids and the evolution of their properties, it is crucial to take into account the large-scale structure where they are embedded (Paranjape, Lam & Sheth 2012).

Essentially, the hierarchy of voids arises by the assembly of matter in the growing nearby structures. Sheth & van de Weygaert (2004) suggest that while some voids remain as underdense regions, other voids fall in on themselves due to the collapse of dense structures surrounding them. According to this scenario, void evolution exhibits two opposite processes, expansion and collapse, the dominant process being determined by the global density around the voids. The distinction between these two types of void behaviours depends on the surrounding environment. It is expected that the large underdense regions with surrounding overdense shells will undergo a 'void-in-cloud' evolution mode. These voids are likely to be squeezed as the surrounding structures tend to collapse on to them.

On the other hand, voids in an environment more similar to the global background density will expand and remain as underdense regions following a so-called 'void-in-void' mode. In this scenario, it could be expected that largest voids at present remain stable, and thus are unlikely to be surrounded by overdense regions that are massive enough to produce a contraction. However, many of the smallest voids at present may show surrounding overdense shells. Inspired by this schematic scenario, we analyse the void-size dependence of the relative population of voids embedded in low-density and overdense regions.

This paper is organized as follows: in Section 2, we describe the galaxy and mock catalogues and the corresponding void catalogues. In Section 3, we provide the analysis of the environments of voids in the Sloan Digital Sky Survey (SDSS). A comparison of observational results to the numerical simulation and the mock catalogue is given in Section 4. Finally, we discuss our results in Section 5.

2 DATA

2.1 Galaxy catalogue and void sample

The observational data used in this work were extracted from the main galaxy sample (Strauss et al. 2002) of the SDSS data release 7 (SDSS-DR7; Abazajian et al. 2009). The SDSS contains CCD imaging data in five photometric bands (*UGRIZ*; Fukugita et al. 1996; Smith et al. 2002). The SDSS-DR7 spectroscopic catalogue comprises in this release 929 555 galaxies with a limiting magnitude of $r \leq 17.77$ mag.

The voids in the galaxy distributions are identified using volume complete samples. We adopt a limiting redshift $z = 0.08$ and maximum absolute magnitude in the r band $M_r = -19.2$. The limiting redshift of the sample is chosen on the basis of a compromise between the quality of the void sample, determined by the dilution

of the sample of galaxies, and the number of voids, required to be large in order to achieve statistically significant results.

We have explored the effects of shot noise on the void identification in both real data and simulations in Ceccarelli et al. (2006). We found that for low-density galaxy samples, the identification of small voids ($R_{\mathrm{void}} < 10\,h^{-1}$ Mpc) is limited by shot noise; however, we can identify voids as small as these in denser galaxy samples that can be obtained by restricting the analysis to low redshifts ($z \lesssim 0.1$ in SDSS).

Our sample is redshift limited to have a large enough galaxy density to avoid the effects of shot noise on small voids (down to $5\,h^{-1}$ Mpc), but also a large enough volume to provide a statistically significant number of objects. We apply the void finding algorithm described in Padilla et al. (2005) and Ceccarelli et al. (2006) to this volume-limited sample. In order to prevent effects of survey geometry and redshift limits on the process of void identification, we avoid including voids near the survey edges. The algorithm identifies the largest spherical regions where the overall density contrast is at most $\Delta = -0.9$, and which are not contained in any other sphere satisfying the same condition. According to this procedure, a void is located at the centre of an underdense sphere and has a scale size equal to the sphere radius. We obtain 131 voids in the SDSS sample with radii ranging from 5 to $22\,h^{-1}$ Mpc.

2.2 Large-scale numerical simulation

We use the snapshot corresponding to $z = 0.0$ of the Millennium simulation (Springel et al. 2005; Lemson & Virgo Consortium 2006) and the associated semi-analytic model of galaxy formation by Bower, McCarthy & Benson (2008). The Millennium simulation utilizes a Λ cold dark matter (ΛCDM) cosmological model with $\Omega_\Lambda = 0.75$, $\Omega_M = 0.25$, $\Omega_b = 0.045$, $h = 0.73$, $n = 1$ and $\sigma_8 = 0.9$ based on *Wilkinson Microwave Anisotropy Probe* observations (Spergel et al. 2003) and 2dF Galaxy Redshift Survey (Colless et al. 2001). The simulation follows the evolution of 2160^3 particles, each with $8.6 \times 10^8\,h^{-1}\,\mathrm{M}_\odot$ through a comoving box of side 500 Mpc. The dark matter haloes of the Millennium simulation were used to follow the simulated growth of galaxies by implementing a semi-analytic model of galaxy formation (GALFORM; Bower et al. 2008), which generates a population of galaxies within the simulation box. We used the full simulation box to identify voids and study the effects of dilution and redshift space distortion in the sample of voids. The semi-analytic galaxy catalogue from the simulation box comprises 2783 voids.

We use a mock catalogue, constructed by selecting galaxies within the simulation box. The mock catalogue is constructed by first positioning an observer in a random position within the numerical simulation box, and then reproducing the selection function and angular mask of the SDSS from this position. This results in a mock catalogue of galaxies of similar properties and observational biases to those of the SDSS catalogue. Positions in real-space and peculiar velocities are available to test possible projection biases and to quantify the effects of redshift space distortions. The mock catalogue also provides information on SDSS photometric magnitudes, star formation rates and total stellar masses, based on computations from the semi-analytic model of galaxy formation (Bower et al. 2008). This mock catalogue will be used in this work to calibrate our statistical methods, to interpret the data and to detect any systematic biases in our procedures. In order to do this, we will treat the mock catalogue in exactly the same way as the real data. We found 113 mock voids, with radii ranging from 5 to $23.75\,h^{-1}$ Mpc.
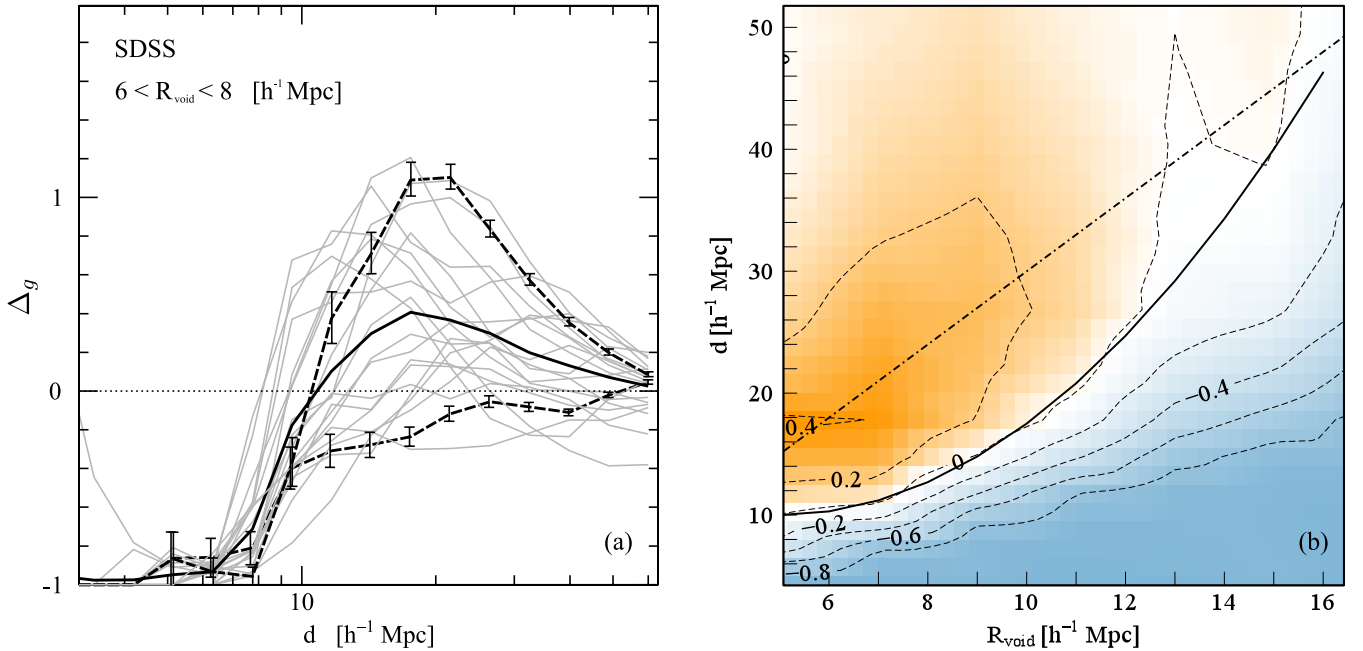
Figure 1. Left-hand panel: integrated galaxy density (Δ_g) as a function of distance to the void centre for individual voids in SDSS with radii in the range of 6–8 h^{-1} Mpc (grey lines). The thick black solid line indicates the mean density contrast profile of all voids. The thick dashed lines show two different profiles: with and without a noticeable maximum in the density profile and the error bars represent the corresponding Poisson errors. Right-hand panel: contour lines of mean density contrast as a function of void radius and distance to the void centre d in SDSS. Orange colours represent positive densities (increasing from light to dark) and cyan correspond to negative densities. Dashed lines represent isodensity contours ($\Delta_g = -0.8, -0.6, -0.4, -0.2, 0, 0.2$ and 0.4) as is labelled in the figure. The solid line represents an approximate fit to the zero-density contour line. The dot–dashed lines indicate the relation $3 \times R_{\text{void}} = d$.

3 LARGE-SCALE REGIONS SURROUNDING VOIDS IN GALAXY CATALOGUE

Sheth & van de Weygaert (2004) proposed that void evolution is strongly determined by the larger regions surrounding them. In this framework, voids embedded in overdense environments tend to experience gravitational collapse more likely than expansion. Consequently, it is expected that most of the small voids with an overdense shell surrounding them have sank inwards by the present epoch. Larger voids, on the other hand, are probably expanding in concordance with the formation of large structures shaping them. We analyse the relative abundance of voids embedded in overdense environments for different void sizes in the galaxy distribution. Such abundances are used in this section to test model predictions about voids in the SDSS spectroscopic galaxy catalogue.

3.1 Void density

Padilla et al. (2005) provide mean relations between the maximum density, its radial distance to the void centre and the void radius. In order to further explore these relations, we study the integrated density contrast profiles of galaxies as a function of the void radius and distance to the void centre. We compute for each void the integrated number density contrast of galaxies, Δ_g, as

$$\Delta_g(d) = \frac{n_g(d) - \langle n \rangle}{\langle n \rangle}, \tag{1}$$

where $\langle n \rangle$ is the mean number density of galaxies in the catalogue and $n_g(d)$ is the number density of galaxies within a void-centred sphere of radius d. In order to compensate for the effects due to the survey limits and geometry on our density calculations, we use appropriate random catalogues to estimate densities.

In the left-hand panel of Fig. 1, we show Δ_g as a function of the void-centric distance (d) for all voids with size (R_{void}) in the range of 6–8 h^{-1} Mpc (grey solid lines). The thick black solid line represents the mean integrated density contrast for this void sub-sample, hereafter $\langle \Delta_g \rangle$. By inspection of this panel, it can be noticed that there is a significant variation of individual curves around the mean. We also highlight with thick dashed lines two profiles that illustrate two distinct behaviours: profiles with a noticeable maximum density contrast and a decline at larger distances; and those showing a non-decreasing profile that tends to the mean density at large distances from the void centres.

In the right-hand panel of Fig. 1, we show $\langle \Delta_g \rangle$ as a function of (R_{void}, d) for voids with radii in the range $5 < R_{\text{void}/h^{-1}\,\text{Mpc}} < 16$. An element in this matrix represents $\langle \Delta_g \rangle$, averaged over voids in a given void-sized bin, integrated up to a given maximum void-centric distance d. Therefore, columns in this matrix are the mean integrated density contrast profile as a function of void size and projected distance. The superimposed dashed lines represent different density contrast levels. The solid line corresponds to a fit to the zero-density contrast isocontour in the range $5 < R_{\text{void}/h^{-1}\,\text{Mpc}} < 16$, shown for future reference (see Section 4). Underdense and overdense regions are shown with different colours, ranging from blue to orange for negative to positive density contrasts, respectively. The white colour corresponds to a zero-density contrast, i.e. regions where the integrated density is equal to the mean global density. This panel shows the general trend of the average behaviour of void profiles depending on void sizes. In the mean, the integrated density contrast profile of small voids exhibits a prominent shell, whereas in the case of large voids there is a smooth behaviour towards the global mean galaxy density.

The results shown in the left-hand panel of Fig. 1 suggest that it is possible to classify voids according to their large-scale

radial density profiles allowing for a subdivision of the void sample into two types of voids. We notice that mean integrated density contrast profiles can be defined for R_{void} intervals. These average curves have a well-defined maximum at a distance d_{max} from the void centre, except for the largest voids that exhibit asymptotically increasing profiles. When there is no clear local maximum, we adopt $d_{max} = 3R_{void}$. This choice is justified by the fact that small- and intermediate-sized voids have $d_{max} \sim 3R_{void}$ (right-hand panel of Fig. 1). Thus, we classify voids into two subsamples according to positive or negative values of the integrated density contrast at d_{max}. Voids surrounded by an overdense shell (hereafter S-type voids) correspond to $\Delta_g(d_{max}) > 0$. On the other hand, R-type voids ($\Delta_g(d_{max}) < 0$) correspond to voids with continuously rising density profiles.

In the left-hand panels of Fig. 2, we show the galaxy density profile for S-type voids with radii in two ranges $6\,h^{-1} < R_{void} < 8\,h^{-1}$ Mpc and $10\,h^{-1} < R_{void} < 12\,h^{-1}$ Mpc. The solid lines correspond to the mean density whereas dots correspond to the individual void profiles. The profiles of R-type voids are shown in the right-hand panel of this figure. The similarity of the inner radial density profiles of S- and R-type voids can be appreciated, regardless of their different large-scale environment. For the total sample of voids, we obtain 59 S-type and 82 R-type voids. The solid lines in the upper panels of Fig. 3 show the cumulative number of voids corresponding to the S-type (left-hand panel) and R-type sample (right-hand panel) in the SDSS catalogue. The opposite trends distinguishing both samples can be noticed: while the quantity of S-type voids decreases as the radius increases, that of R-type voids monotonically increases. This is consistent with the theoretical results indicating that large voids are unlikely to be surrounded by overdense shells (Paranjape et al. 2012).
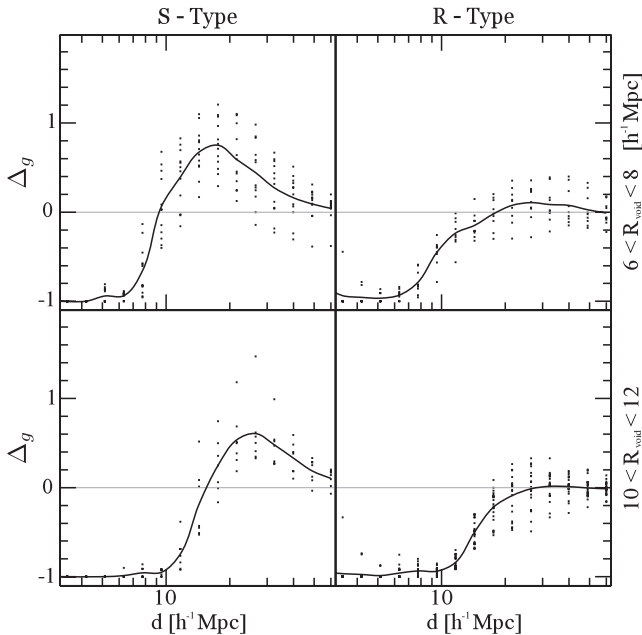

Figure 3. Upper panels: integrated number of voids as a function of radius in SDSS (solid lines, filled circles) and in the mock (dashed lines, open circles) catalogues, for voids with (S-type) and without (R-type) a surrounding overdense shell (left- and right-hand panels, respectively). Lower panels: fraction of the total volume occupied by voids smaller than R_{void}^{max}, for voids with and without a surrounding overdense shell in SDSS (solid lines, filled circles) and in the mock (dashed lines, open circles) catalogues.

The relative volume occupied by voids smaller than a given maximum void radius R_{void}^{max} is shown in the lower panels of Fig. 3, for S- and R-types separately. As can easily be seen in the lower-left panel, approximately 10 per cent of the catalogue is occupied by S-type voids (solid lines, filled dots). On the other hand, the volume occupied by R-type voids increases with radius (solid lines, filled dots in the lower-right panel of Fig. 3) and they approximately occupy half of the total volume, in agreement with the well-known statement that most of the volume of the Universe is filled by voids.

3.2 Fraction of S- and R-type voids

In this subsection, we analyse the fraction of S- and R-type voids as a function of void radius. The results are displayed in Fig. 4 for SDSS data and the results of the mock catalogue (discussed in Section 4). Error bars correspond to the 68 per cent confidence interval of the binomial distribution. It can be seen in this figure that most of the smallest voids are surrounded by an overdense region while larger voids tend to have smoothly rising density profiles. A similar behaviour has been reported by Sheth & van de Weygaert (2004), based on a void sample identified in numerical simulations. They provide a theoretical framework based on the excursion set formalism where the void population is twofold, according to their evolutionary processes. Our classification of void's density profiles resembles the idea of a void-in-void and void-in-cloud dichotomy in the evolutionary processes presented by Sheth & van de Weygaert (2004). We have found that the relative number of voids in S-type decreases as the size increases. The comparison with simulation results is detailed in the next section.

Figure 2. Integrated density contrast profiles around voids of radii in the ranges of 6–8 h^{-1} Mpc (upper panels) and 10–12 h^{-1} Mpc in SDSS (lower panels). The profiles in the left-hand panels correspond to voids surrounded by overdense shells, i.e. S-type voids. Right-hand panels are for R-type voids, showing a non-decreasing or 'rising' profile. The solid thick lines correspond to the mean density contrast profiles and black dots show the values of density contrast for each individual void as a function of distance. The dotted lines indicate the mean galaxy density, i.e. zero-density contrast.
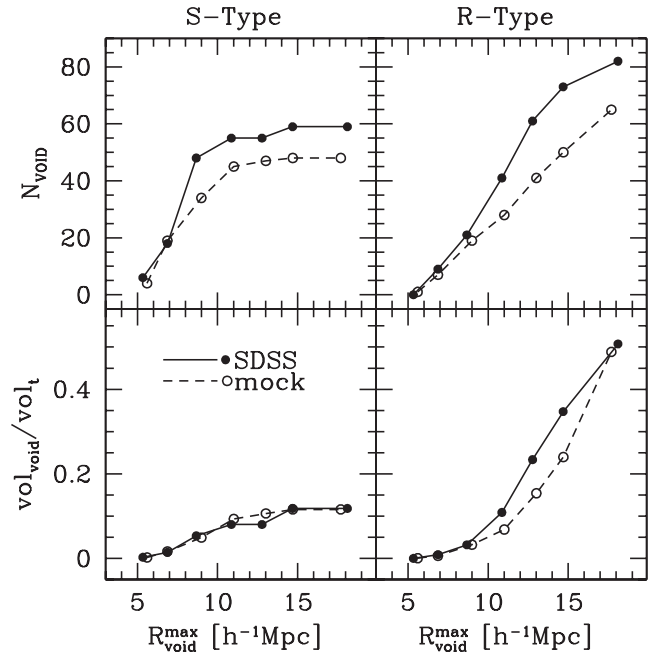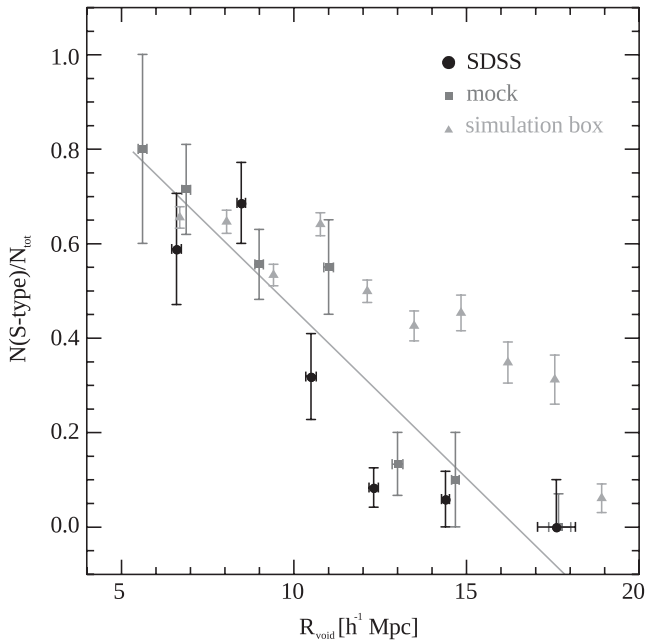
Figure 4. Fraction of S-type voids as a function of void radius. The filled dots represent the fractions for the SDSS sample, grey boxes the corresponding fractions obtained in the mock sample and grey triangles the values computed in the simulation box, in real space. The solid line indicates the linear regression fit to SDSS data. Error bars represent the 68 per cent confidence interval of the binomial distribution.

4 ΛCDM COMPARISON

In this section, we use the mock catalogue constructed using the numerical simulation, and identify and classify voids using the same methods as applied to the observations in the previous sections. The Millennium simulation, described in Section 2, provides three-dimensional positions and velocities of semi–analytic galaxies. This allows us to analyse the properties of voids defined by galaxy positions for different types of large-scale surrounding regions. The simulation and the mock catalogue can also be used to test possible systematics in the definition and properties of voids, which can change from real to redshift space (Ryden & Melott 1996; Schmidt, Ryden & Melott 2001).

With the aim to compare the results of galaxy catalogue to numerical results, we study the behaviour of the void integrated density profiles $\Delta_g(d)$ as a function of both void radius (R_{void}) and void-centric distance (d), in the mock catalogue and in the simulation box. The semi-analytic sample of galaxies comprises all galaxies from the $500\,h^{-1}$ Mpc^3 simulation box. As is described in Section 2.2, the mock galaxy catalogue is constructed from the semi-analytic sample of galaxies, and with the same angular mask and redshift space effects than the SDSS spectroscopic galaxy catalogue. This allows a better understanding of the spread in the behaviours of the different void profiles. In panels (a) and (c) of Fig. 5, we show the integrated galaxy overdensity profiles of voids with sizes ranging 6–8 h^{-1} Mpc in both, the mock catalogue and the simulation box. In order to avoid shot noise in the estimation of the density profile, we require galaxy counts to be above 100 in each radial distance bin. Due to this limitation, the curves are trimmed at small radial distances. As can be seen in panel (a), the individual curves span a wide range of behaviours for the galaxy number overdensity Δ_g as a function of centre–void distance d. Similar features are observed, although with better coverage, in the sample of voids in the simula-

tion box (panel c of Fig. 5). Given the high number of voids found in the simulation volume, we show just a random subset of void profiles (grey lines). The curves can again be subdivided in groups showing two behaviours: that of a prominent maximum indicating the presence of an averaged overdensity in a surrounding shell and the characteristic smooth rise to $\Delta = 0$ at large distances. In order to illustrate these distinct behaviours, the black dashed lines in panel (a) show the profiles of two voids that are clearly classified into S- and R-types. The black solid line in both panels, (a) and (c), represents the mean integrated density profile $\langle \Delta_g \rangle$ of the mock and simulation samples, respectively. In the case of the simulation box, due to the larger volume covered, the number of voids in the sample is larger, allowing a more detailed analysis of the behaviour of void profiles. For instance, in panel (c) the colour map represents a 2D histogram of the number of voids in bins of the integrated galaxy density profile (Δ_g) and the void-centric distance (d), where redder colours indicate higher number counts and blue colour accounts for one measurement in that bin. As can be seen, the lack of red coloured bins at separations $<30\ h^{-1}$ Mpc shows that the distribution of overdensity values becomes broader. It should be noticed that each curve is sampled at a discrete set of values for the void-centric distance (the bins in d), giving rise to the noisy aspect of the colour map for low-density values.

In the above paragraph, we have illustrated for a fixed range of void sizes (6–8 h^{-1} Mpc) the features observed in void profiles. We also provide in Fig. 5 an analysis of the mean void density profile $\langle \Delta_g \rangle$ as a function of void size. This is shown in panels (b) and (d), where mean galaxy overdensity is presented as a function of the void radius (R_{void}) and the distance to the void centre (d) in the mock catalogue and in the simulation box, respectively. Orange colours represent overdense regions ($\langle \Delta_g \rangle > 0$), whereas cyan colours correspond to underdense regions (negative overdensities). The dashed lines represent isodensity contours as labelled in the figure. The solid lines in both panels represent an approximation to the $\Delta_g = 0$ isodensity contour in the mock sample, also shown for comparison in the simulation sample (panel d). As it can be noticed, small voids tend to exhibit a surrounding overdense shell in their mean profile, whereas larger voids ($10 \lesssim R_{void}$) show continuously rising mean density profiles. It is worth to mention that all the observational effects taken into account in the construction of the mock catalogue do not seem to affect in an appreciable way the mock results. This arises from comparing the mock results (upper panels in Fig. 5) with the simulation results (lower panels).

In order to examine cosmic variance effects on our results, we have also constructed several mock catalogues by placing observers in unconnected locations in the simulation box. We examine the density profiles around voids. In general, they show similar behaviour with small differences between different mocks which are comparable to the difference between mock and observational data (see Figs 1 and 5). We stress on the fact that our theoretical results are in good agreement with observations as can be seen when comparing to Fig. 1.

We select S- and R-type void samples in the mock catalogue following the same criteria described in Section 3 obtaining 48 and 65 S- and R-type voids, respectively. The density profiles corresponding to S- and R-type voids are shown in Fig. 6 (left- and right-hand panels, respectively). In Fig. 4, we present the fraction of S- and R-type voids with respect to the total number as a function of void size in the mock catalogue, where the squares indicate the fraction and error bars represent the confidence interval of the binomial distribution. It is relevant that the mock behaviour is indistinguishable from the observations. We also show the results obtained selecting
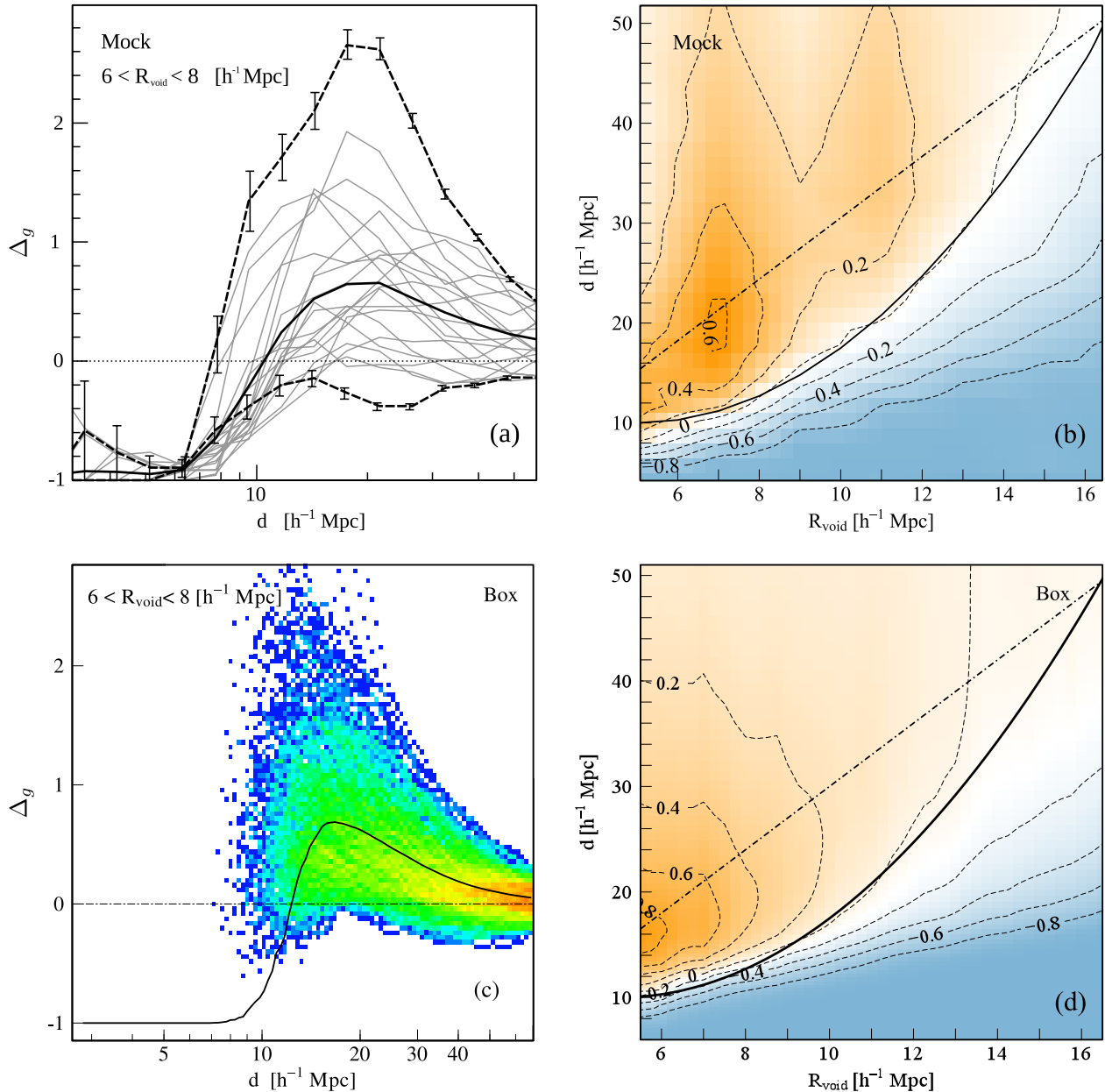
Figure 5. Left-hand panels (a and c): integrated galaxy density profiles (Δ_g, grey lines) of individual voids with sizes between 6 and 8 h^{-1} Mpc, as a function of distance to the void centre (d) for voids in the mock catalogue (panel a) and in a random subset of voids in the simulation (panel c). The black solid lines represent the mean integrated density profile, $\langle \Delta_g \rangle$, in both panels. The black dashed lines in panel (a) correspond to the profiles of two voids that are classified clearly into S- and R-types. The error bars indicate the corresponding Poisson errors. The colour map in panel (c) is the histogram of the number of voids in bins of integrated galaxy density (Δ_g) and void centre distance (d) (redder colours for higher counts). Right-hand panels (b and d): contour lines of mean density, $\langle \Delta_g \rangle$, as a function of the void radius R_{void}, and the distance to the void centre d, in the mock catalogue (panel b) and in the simulation box (panel d). The orange colours represent positive densities (increasing from white) and cyan correspond to negative densities. The dashed lines represent isodensity contours ($-0.8, -0.6, -0.4, -0.2, 0, 0.2, 0.4, 0.6$ and 0.8). The solid lines represent an approximation to the $\Delta_g = 0$ isodensity contour in the mock sample and the dot–dashed line indicates the relation $3 \times R_{void} = d$, also shown for comparison in panel (d).

galaxies brighter than $M_r = -19.2$ in the simulation box (triangles in Fig. 4). Thus, this sample of simulated galaxies has the same absolute limiting magnitude than the volume-complete samples of SDSS and mock galaxies.

Based on analytical formulations for the evolution of inhomogeneities on the mass distribution in the Universe (e.g. Peebles 1993) and the theoretical analysis of void evolution (Sheth & van de Weygaert 2004), it is natural to expect a dependence of the peculiar velocity field around voids with the presence of a surrounding

overdense shell. In order to examine this effect, we have studied the mean peculiar velocity around voids traced by the semi-analytic galaxies in the full simulation box, for S- and R-type voids separately. In Fig. 7, we show the mean velocity profiles of these two subsamples of voids in the mock catalogue, where the dashed line indicates S-type and the solid line the R-type voids. We adopt positive velocities to indicate expansion and negative velocities for infall motions. As can be seen in the figure, S-type voids show substantial infall velocities (rising to -150 km s^{-1}) at the same distances
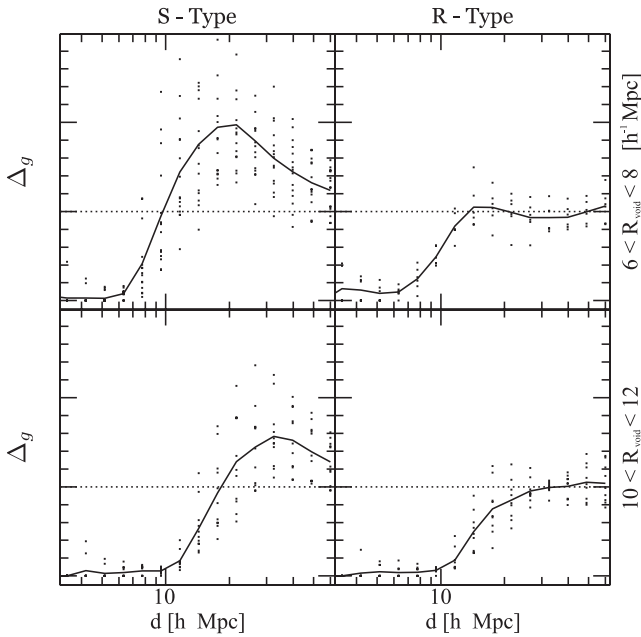
Figure 6. Radial integrated density profile around voids in the mock catalogue with void radii in the ranges of 6–8 h^{-1} Mpc (upper panels) and 10–12 h^{-1} Mpc (lower panels). The left-hand panels correspond to voids surrounded by large-scale overdense shells and the right-hand panels correspond to voids in large-scale underdense regions. The solid lines correspond to the mean density and dots show the individual voids. The dotted lines indicate the mean galaxy density.
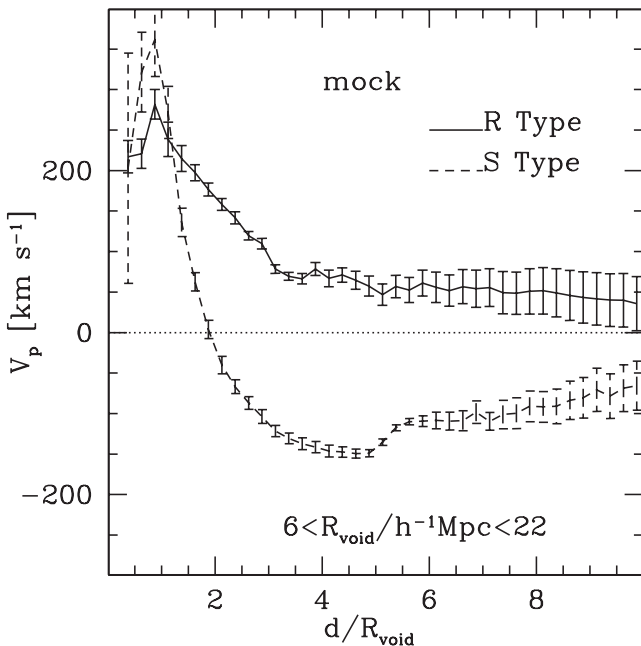

Figure 7. Mean radial velocity profile for voids surrounded (dashed line) and not surrounded (solid line) by overdense shells in the mock catalogue. Void radii are in the range of 6–22 h^{-1} Mpc. The dotted line indicates a zero mean velocity ($v = 0$ km s^{-1}).

where the overdense shells are located ($d/R_{\rm void} \sim 3$) whereas at smaller distances ($d/R_{\rm void} \lesssim 2$) the velocity field is characterized by expansion. On the other hand, R-type voids, lacking an overdense shell, show only expansion velocities. Both samples show signifi-

cant expansion velocities at void shells ($0.8 \leq d/R_{\rm void} \leq 1.2$), with a maximum (velocities ~ 300 km s^{-1}) reached at $d/R_{\rm void} \simeq 1$.

5 SUMMARY AND DISCUSSION

We have performed a statistical study of the void phenomenon focusing on void environments. We have examined the distribution of galaxies around voids in the SDSS, by computing the integrated density contrast profile. There is a correlation between the void-centric distance to the shell of maximum density and the void radius. We defined separation criterion to characterize voids according to their surrounding environment, giving rise to S-type (shell) and R-type (rising) voids. We found that small voids are more frequently surrounded by overdense shells. On the other hand, larger voids are more likely classified as R-type, i.e. with a non-decreasing integrated density contrast profile, which smoothly rises towards the mean galaxy density. The fraction of voids surrounded by overdense shells continuously decreases as the void size increases.

In order to test and interpret the observed properties of voids, we identified and analysed voids in a numerical simulation with a semi-analytic galaxy catalogue. We used the same procedures than those applied to the observational galaxy catalogue to identify and analyse voids, particularly when using the mock catalogue. We have computed the velocity curves for the two types of voids, in the full box and in the mock sample. The results suggest that there is a relation between our separation criterion and the evolution of voids, as was suggested previously by Sheth & van de Weygaert (2004). Good agreement obtained between the SDSS voids sample and the mock catalogue provides additional support to the viability of a ΛCDM model to reproduce the large-scale structure of the Universe as defined by the void network. In this work, we give the first observational evidence of multiple modes in the void hierarchy, which have been predicted in numerical simulations, see for example Paranjape et al. (2012), and references therein.

(LAMOST), Los Alamos National Laboratory, the Max-Planck-Institute for Astronomy (MPIA), the Max-Planck-Institute for Astrophysics (MPA), New Mexico State University, Ohio State University, University of Pittsburgh, University of Portsmouth, Princeton University, the United States Naval Observatory and the University of Washington.

The Millennium simulation data bases used in this paper and the web application providing online access to them were constructed as part of the activities of the German Astrophysical Virtual Observatory.

Some of the plots presented in this work were made by using R software.

REFERENCES

Abazajian K. N. et al., 2009, ApJS, 182, 543
Aikio J., Maehoenen P., 1998, ApJ, 497, 534
Aragon-Calvo M. A., Szalay A. S., 2013, MNRAS, 428, 3409
Aragon-Calvo M. A., van de Weygaert R., Araya-Melo P. A., Platen E., Szalay A. S., 2010, MNRAS, 404, L89
Benson A. J., Hoyle F., Torres F., Vogeley M. S., 2003, MNRAS, 340, 160
Bertschinger E., 1985, ApJS, 58, 1
Biswas R., Alizadeh E., Wandelt B. D., 2010, Phys. Rev. D, 82, 23002
Blumenthal G. R., da Costa L. N., Goldwirth D. S., Lecar M., Piran T., 1992, ApJ, 388, 234
Bos E. G. P., van de Weygaert R., Dolag K., Pettorino V., 2012a, MNRAS, 426, 440
Bos E. G. P., van de Weygaert R., Ruwen J., Dolag K., Pettorino V., 2012b, preprint (arXiv:1211.3249)
Bower R. G., McCarthy I. G., Benson A. J., 2008, MNRAS, 390, 1399
Ceccarelli L., Padilla N. D., Valotto C., Lambas D. G., 2006, MNRAS, 373, 1440
Ceccarelli L., Padilla N., Lambas D. G., 2008, MNRAS, 390, L9
Ceccarelli L., Herrera-Camus R., Lambas D. G., Galaz G., Padilla N. D., 2012, MNRAS, 426, L6
Clampitt J., Cai Y.-C., Li B., 2013, MNRAS, 431, 749
Colberg J. M., Krughoff K. S., Connolly A. J., 2005a, MNRAS, 359, 272
Colberg J. M., Sheth R. K., Diaferio A., Gao L., Yoshida N., 2005b, MNRAS, 360, 216
Colberg J. M. et al., 2008, MNRAS, 387, 933
Colless M. et al., 2001, MNRAS, 328, 1039
Einasto M., Tago E., Jaaniste J., Einasto J., Andernach H., 1997, A&AS, 123, 119
Einasto M. et al., 2012, A&A, 542, 36
El-Ad H., Piran T., 1997, ApJ, 491, 421
El-Ad H., Piran T., 2000, MNRAS, 313, 553
El-Ad H., Piran T., Dacosta L. N., 1997, MNRAS, 287, 790
Fillmore J. A., Goldreich P., 1984, ApJ, 281, 9
Frisch P., Einasto J., Einasto M., Freudling W., Fricke K. J., Gramann M., Saar V., Toomet O., 1995, A&A, 296, 611
Fukugita M., Ichikawa T., Gunn J. E., Doi M., Shimasaku K., Schneider D. P., 1996, AJ, 111, 1748

Furlanetto S. R., Piran T., 2006, MNRAS, 366, 467
Hahn O., Porciani C., Carollo C. M., Dekel A., 2007a, MNRAS, 375, 489
Hahn O., Carollo C. M., Porciani C., Dekel A., 2007b, MNRAS, 381, 41
Hausman M. A., Olson D. W., Roth B. D., 1983, ApJ, 270, 351
Hernandez-Monteagudo C., Smith R. E., 2012, preprint (arXiv:1212.1174)
Hoffman Y., Shaham J., 1982, ApJ, 262, L23
Hoyle F., Vogeley M. S., 2002, ApJ, 566, 641
Hoyle F., Vogeley M. S., 2004, ApJ, 607, 751
Icke V., 1984, MNRAS, 206, 1P
Kauffmann G., Fairall A. P., 1991, MNRAS, 248, 313
Kolokotronis V., Basilakos S., Plionis M., 2002, MNRAS, 331, 1020
Lavaux G., Wandelt B. D., 2010, MNRAS, 403, 1392
Lemson G., Virgo Consortium t., 2006, preprint (astro-ph/0608019)
Lietzen H., Tempel E., Heinmki P., Nurmi P., Einasto M., Saar E., 2012, A&A, 545, 104
Mathis H., White S. D. M., 2002, MNRAS, 337, 1193
Melott A. L., Shandarin S. F., 1990, Nat, 346, 633
Müller V., Arbabi-Bidgoli S., Einasto J., Tucker D., 2000, MNRAS, 318, 280
Neyrinck M. C., 2008, MNRAS, 386, 2101
Padilla N. D., Ceccarelli L., Lambas D. G., 2005, MNRAS, 363, 977
Pan D. C., Vogeley M. S., Hoyle F., Choi Y.-Y., Park C., 2012, MNRAS, 421, 926
Paranjape A., Lam T. Y., Sheth R. K., 2012, MNRAS, 420, 1648
Park C., Choi Y.-Y., Kim J., Gott J. R., Kim S. S., Kim K.-S., 2012, ApJ, 759, L7
Patiri S. G., Betancort-Rijo J. E., Prada F., Klypin A., Gottlöber S., 2006, MNRAS, 369, 335
Peebles P. J. E., 1993, Principles of Physical Cosmology. Princeton Univ. Press, Princeton, NJ
Peebles P. J. E., 2001, ApJ, 557, 495
Pellegrini P. S., da Costa L. N., de Carvalho R. R., 1989, ApJ, 339, 595
Platen E., van de Weygaert R., Jones B. J. T., 2008, MNRAS, 387, 128
Plionis M., Basilakos S., 2002, MNRAS, 330, 399
Ryden B. S., Melott A. L., 1996, ApJ, 470, 160
Schmidt J. D., Ryden B. S., Melott A. L., 2001, ApJ, 546, 609
Shandarin S., Feldman H. A., Heitmann K., Habib S., 2006, MNRAS, 367, 1629
Sheth R. K., van de Weygaert R., 2004, MNRAS, 350, 517
Slezak E., de Lapparent V., Bijaoui A., 1993, ApJ, 409, 517
Smith J. A. et al., 2002, AJ, 123, 2121
Spergel D. N. et al., 2003, ApJS, 148, 175
Springel V. et al., 2005, Nat, 435, 629
Strauss M. A. et al., 2002, AJ, 124, 1810
Sutter P. M., Lavaux G., Wandelt B. D., Weinberg D. H., 2012a, ApJ, 761, 44
Sutter P. M., Lavaux G., Wandelt B. D., Weinberg D. H., 2012b, ApJ, 761, 187
Tikhonov A. V., 2006, Astron. Lett., 32, 727
van de Weygaert R., Bertschinger E., 1996, MNRAS, 281, 84
White S. D. M., 1979, MNRAS, 186, 145

This paper has been typeset from a TEX/LATEX file prepared by the author.